

## Mo-99 2011 — MOLYBDENUM-99 TOPICAL MEETING

December 4-7, 2011  
La Fonda Hotel  
Santa Fe, New Mexico

### Development Activities in Support of Accelerator Production of $^{99}\text{Mo}$ Production through the $\gamma/n$ reaction on $^{100}\text{Mo}$

P. Tkac, S. Chemerisov, V. Makarashvili and G. F. Vandegrift  
Chemical Sciences and Engineering Division  
Argonne National Laboratory, 9700 South Cass Ave., 60439 Argonne, IL – USA

and

J. Harvey  
NorthStar Medical Radioisotopes  
706 Williamson St, 53703 Madison, WI – USA

#### ABSTRACT

One of the proposed accelerator-based  $^{99}\text{Mo}$  production pathways uses the photonuclear reaction  $^{100}\text{Mo}(\gamma,n)^{99}\text{Mo}$  in an enriched  $^{100}\text{Mo}$  target (NorthStar Medical Radioisotopes, LLC). Several scaled production experiments have been performed. Last April, the ability to cool a Mo-disk target with power deposition up to 1 kW per disk was demonstrated using He gas at 300 psi. Based on those results, a new He cooling loop was developed by Los Alamos National Laboratory, and full-scale demonstration of the irradiation of a production-scale target is planned for the first quarter of next year. To better mimic plant scale irradiation, the Mo target will be irradiated simultaneously from two opposite sides. To accomplish that, a new dual beamline was developed and is now under construction at the electron linear accelerator facility at Argonne. The linac is undergoing an upgrade to increase beam energy to 35 MeV for more efficient  $^{99}\text{Mo}$  production. Extraction of  $^{99m}\text{Tc}$  from low-specific-activity Mo feed is accomplished by using the NorthStar  $^{99}\text{Mo}/^{99m}\text{Tc}$  generator. Dissolution of Mo target disks is performed using 30% hydrogen peroxide. From dissolution studies, it is becoming evident that the packing density and the sintering process are the most significant factors affecting dissolution rates.

#### 1. Introduction

The National Nuclear Security Administration's (NNSA's) Global Threat Reduction Initiative (GTRI), in partnership with commercial entities and the US national laboratories, is working to address the need for a reliable domestic supply of  $^{99}\text{Mo}$  for nuclear medicine while also

minimizing the civilian use of HEU. This paper discusses the activities performed at Argonne National Laboratory (ANL) in collaboration with Los Alamos National Laboratory (LANL) and NorthStar Medical Radioisotopes that support the accelerator production technology pathway for the production of  $^{99}\text{Mo}$  using photonuclear reaction  $^{100}\text{Mo}(\gamma,n)^{99}\text{Mo}$  in an enriched  $^{100}\text{Mo}$  target. A plot of the photonuclear cross section for this reaction is shown in Figure 1. The threshold for the reaction is 9 MeV. The maximum cross section is 150 mb at 14.5 MeV. Enriched  $^{100}\text{Mo}$  for the targets is commercially available from several vendors for \$400 to \$600 per gram.

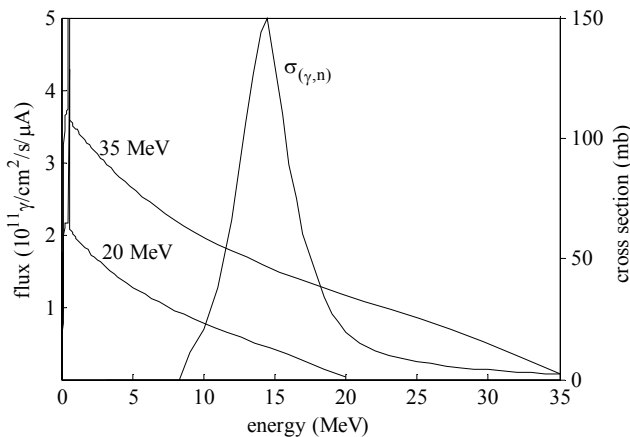


**Figure 1.** Photonuclear cross section of  $^{100}\text{Mo}$  and average bremsstrahlung photon spectra produced with a 20- and 35-MeV electron beam in a molybdenum target.

In this approach a high-power electron accelerator is used to produce the required flux of high-energy photons through bremsstrahlung process. The bremsstrahlung photon output spectra from 20- and 35-MeV electron beams incident on a molybdenum target are shown compared with the  $^{100}\text{Mo}$  photo-neutron spectra in Figure 1. In FY 2010 we have performed three demonstration of the  $^{99}\text{Mo}$  production in the natural and enriched  $^{100}\text{Mo}$  utilizing liquid (water) cooling approach. Those experiments have demonstrated production of the  $^{99}\text{Mo}$  at relatively low beam power on the target and effective separation of the  $^{99\text{m}}\text{Tc}$  from low specific activity targets, but they also pointed out limitations of the liquid cooling and corrosion/erosion of the Mo target in water under high radiation field. To eliminate problem associated with water cooling and extend power envelope on the target we have decided to utilize gaseous He cooling. In March 2011 ANL and LANL scientists have successfully demonstrated ability to dissipate up to 1 kW power per 12 mm diameter 1 mm thick disk using He one through flow system (300 sqf/min). This way of cooling is limiting the time of the irradiation to several minute. To extend irradiation time to multiple hours or days the concept of the closed loop He cooling system was developed and thermal and production tests using He cooled target are planned for the beginning on calendar year 2012.

## 2. Experimental set-up

### *Dissolution of Mo disks*

Since the final Mo solution to be used in the NorthStar generator needs to be highly alkaline, the focus for the dissolution studies was to develop a technique that would produce a solution of molybdate easily convertible or already prepared in sodium or potassium hydroxide. Several methods for the dissolution of Mo metallic and sintered discs were investigated: (1) dissolution in NaOH at elevated temperature, (2) electrochemical dissolution in NaOH, and (3) dissolution

in 30% H<sub>2</sub>O<sub>2</sub>. This paper focuses on the dissolution data of Mo 12mm×1mm sintered disks using hydrogen peroxide. Usual conditions for the dissolution of disks (~1.1g per disk) were ~40mL of 30% H<sub>2</sub>O<sub>2</sub> with starting temperature ~70°C, if not stated otherwise. Addition of Mo sintered disk(s) into the solution of 30% H<sub>2</sub>O<sub>2</sub> lead to a rapid increase of the temperature (~100°C) and leads to a very strong reaction with strong bubble and gas formation. In general, the disks with smaller packing density provide stronger reaction than the disks with higher densities. To prevent splattering, the volume of H<sub>2</sub>O<sub>2</sub> used should be less than 20% of the volume of beaker or container used for the dissolution.

### *Separation of Mo and Tc*

Separation processing of the solution containing high concentration of Mo and only tracer quantities of <sup>99m</sup>Tc require a different approach compared to the one usually used in commercial Mo/Tc generators with high specific activity of <sup>99</sup>Mo. The chemical separation of <sup>99m</sup>Tc from <sup>99</sup>Mo/Mo on the NorthStar generator relies on the highly selective resin. The solution containing Mo in (Na/K)OH, with the <sup>99m</sup>Tc at some level of ingrowth is initially passed through the Primary Capture Resin (ABEC®) which selectively captures the <sup>99m</sup>Tc while passing the molybdenum into the parent recovery vessel (see Figure 2). After a rinse of the Primary Capture Resin (PCR) with hydroxide followed by a rinse with acetic acid/acetate buffer solution, the <sup>99m</sup>Tc is stripped from the PCR with normal saline solution. The eluted <sup>99m</sup>Tc is passed through the Guard Alumina column (GC), which is selective (under the strip conditions) for any Mo(VI) that may be present. The use of the GC is equivalent to a second purification step of the final <sup>99m</sup>Tc product from the parent radioisotope. The purified <sup>99m</sup>Tc is captured in the daughter receiving vessel in ~5mL of normal saline solution.

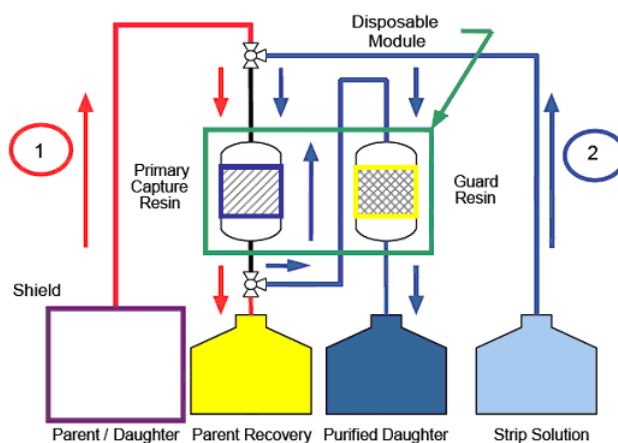


**Figure 2.** Scheme of <sup>99m</sup>Tc/<sup>99</sup>Mo separation with NorthStar generator

## **3. Results and Discussion**

### **3.1. Activities related to the production of Mo-99**

#### *Development of the beam line for two sided irradiation*

Most of the heat deposited on the target is dissipated in the first centimeter of the target material while production of the <sup>99</sup>Mo is distributed more evenly. One can achieve a higher total concentration of <sup>99</sup>Mo by irradiating a Mo target from two sides while maintaining the same thermal load per unit length of the target. We can irradiate the target from both sides by splitting the incoming electron beam into two components. This can be done with a magnetic dipole, which will bend the incoming beam 10 degrees for a prescribed amount of time. This component

of the beam must pass through a beam line consisting of several deflecting and focusing elements such that it arrives at the target from one side. When the magnetic dipole is not powered the electron beam goes straight and arrives at the target from the other side. The maximum frequency of beam “chopping” is about 300Hz. A realistic beamline arrangement is shown in Figure 3. The transport beamline shown contains a second magnetic dipole (identical with the first one), which bends the beam with -10 degrees, an alpha-magnet, which bends the beam with 270 degrees and two 45-degree magnets, which bend the beam with 45 degrees each.

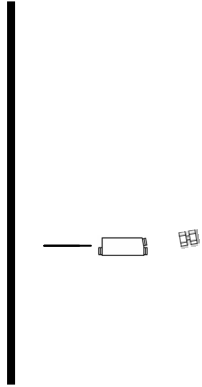


**Figure 3.** Beamline design for two-sided irradiation

The particle tracking code Impact-T propagates the initial ensemble of macroparticles through the entire beamline with a predefined timestep. Typically the timestep should be much shorter than the rf-period. In our case the rf-period is 769 ps and the timestep is 1 ps. The code outputs the beam moments (like beam transverse and longitudinal sizes, energy spread, number of lost particles, angular spread, etc.) at each timestep and more complete information like the particle distribution, at any required position along the beamline. During the beam propagation, the code computes at each timestep the external forces, in this case magnetic forces due to the dipoles and quadrupoles, and the internal forces due to collective effects. These forces are evaluated at the position of each macroparticle and the new positions are calculated assuming that forces are constant during the time step. By default, the only collective effect taken into account by Impact-T is related to the repulsive space charge forces between any electron pair in the bunch. We determined that space charge forces are negligible in this case due to the relatively small bunch charge and to the ultra-relativistic regime. During the passage of an electron between the poles of a magnet, the electron is deflected by a certain angle in the horizontal plane dependent on its energy and the magnitude of the magnetic field. A large beam energy spread produces large angular divergence in x-direction. In order to compensate this effect, several quadrupoles are used to focus the beam.

The diameter of the beampipe (2") and the relatively small geometrical acceptances of the alpha-magnets and the 45-degree magnets require a good beam focusing all the way along the beamline and not just at the target. Therefore, the quadrupoles are used whenever space constraints allow it. The field gradients in the quadrupoles were optimized to yield a maximum transmission coefficient and also to maximize the percentage of the beam that is focused within a 5.0 mm circle at the target. In the case shown in Figure 4 almost the entire beam (99.4%) can be focused within this circle. The most critical parameter is the energy spread, which we have measured to be close to 1%. The rectangular shape of the transverse distributions at the entrance of the alpha-magnet (Figure 5) is determined by the beam focusing with the first eight quadrupoles and the

requirement that the beam fits within the rectangular magnet aperture. When the energy spread in the simulation is raised to 2%, about two times more than expected, the beam focusing becomes a lot harder. Even though the transmission coefficient is still high (96%), only about 86% of the beam can be focused within the 5.0 mm circle at the target. To make transport system more tolerant to the beam energy we have rearranged beamline components to minimize the path after 10 degree bend. The final layout for beam transport system is shown in Figure 6.

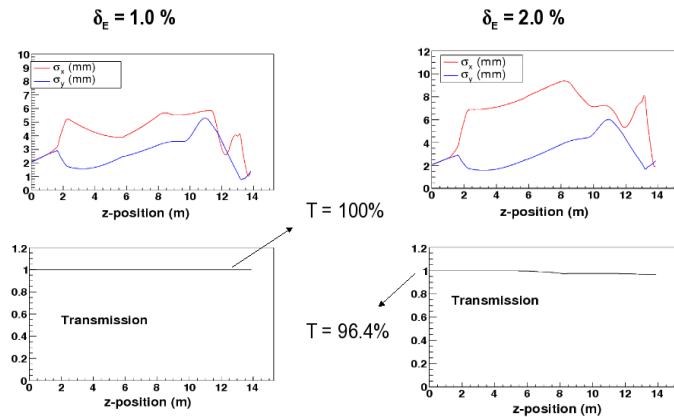


**Figure 4.** Beam envelopes and transmission coefficients for beamline containing one alpha and two 45-degree magnets are used and energy spread is 1% (left) and 2% (right).

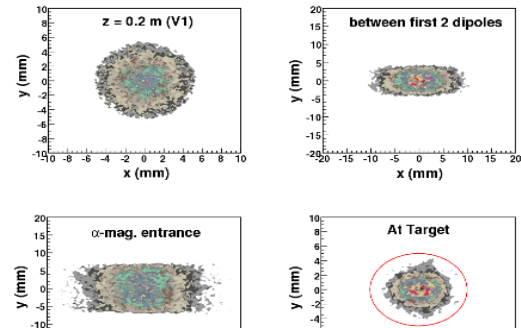


**Figure 5.** Transverse beam projections at four locations for a beamline containing two 45-degree magnets and energy spread at 1%. About 99% of the beam is focused within the 5.0 mm radius circle at the target.

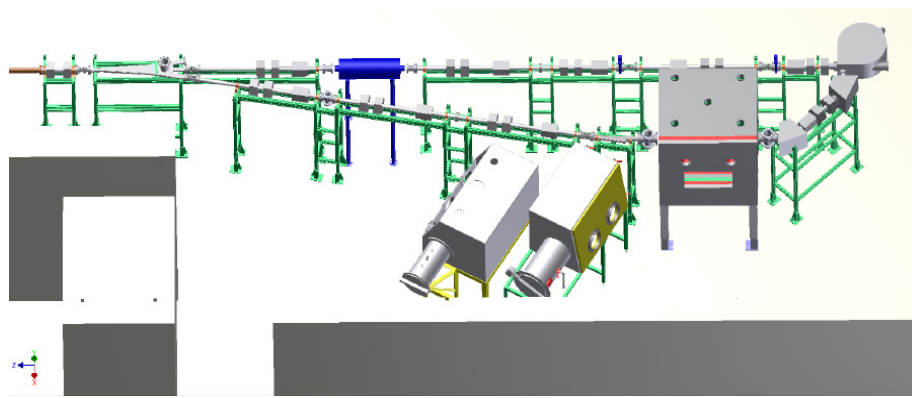


**Figure 6.** New beam line layout for two sided irradiation of the Mo target. Target will be located in the middle of the shielded box

*Computer simulation for full scale production target*

Proposed LINAC based  $^{99}\text{Mo}$  production experiments were simulated with a Monte Carlo particle transport code called MCNPX. These full scale experiments involve a closed loop helium cooling system with target consisting of 25 molybdenum disks. Both natural Mo and

100%  $^{100}\text{Mo}$  enriched targets were studied computationally. Natural disks were chosen for heating studies while enriched disks will be used during production phase experiments. Disks are 12 mm diameter and 1 mm thick. They are placed in a housing made out of Inconel-718 alloy. The housing has an inlet and an outlet on the sides for helium flow. The target was developed at LANL. MCNPX simulations were performed to study heating and  $^{99}\text{Mo}$  production profiles for 16, 18, 20 and 35 MeV beam energies for a natural molybdenum target and 20 and 35 MeV for a 100% enriched  $^{100}\text{Mo}$  target. Two sided irradiation experiment was also simulated for a 35 MeV beam and a natural molybdenum target. Heating profile results are shown in Figure 7 for one sided and two sided irradiations. Production profiles for natural Mo disks are presented in Figure 8, which shows total production for each disk for both – one and two sided irradiations.

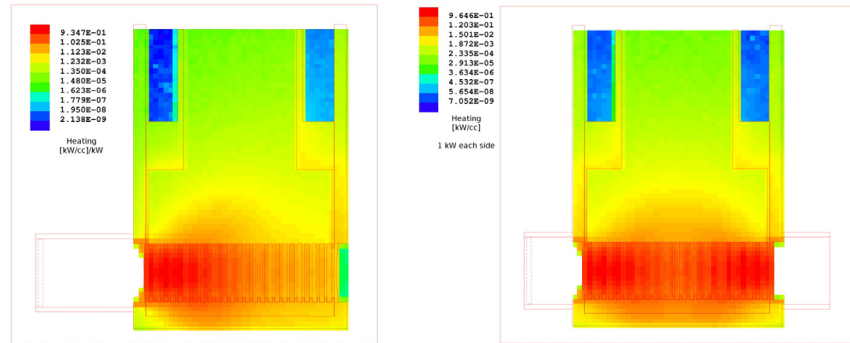


**Figure 7.** Power density distribution [ $\text{kW}/\text{cm}^3$ ] per kW of beam power for a 35 MeV beam on natural molybdenum disks. One sided and two sided irradiations are simulated with MCNPX.

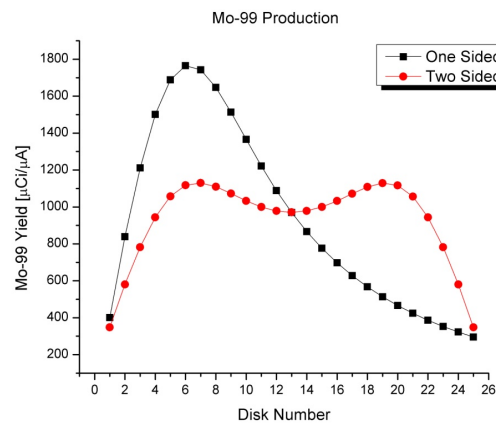


**Figure 8.** Total production per disk [ $\mu\text{Ci}/\mu\text{A}$ ] for one and two sided irradiations at 35 MeV electron beam energy on natural Mo target

#### *Effects of the misalignment of the beam on the target*

Alignment of the beam with the target has become a very important issue not only for our experiments, but also for development of the alignment/beam monitoring system for production target. In production facility direct access to the target would not be possible due to high radiation fields present from activated beam components and shielding. Optical Transition Radiation (OTR) can be used to monitor position of the beam at the exit window or from face of the target housing. With the current design of the target and target housing OTR image can be the way to assure proper alignment of the beam to the target because target housing also serves

as the beam window and housing wall is also located very close (1 mm) from the Mo target itself. Beam can be easily aligned to the center of the window in vertical and horizontal direction the only concern is that in this arrangement electron beam would be not necessary perpendicular to face of the target. In following simulations we have addressed possible experimental issue of striking the target with an angled beam. 1 to 7 degree angular deviations (with 1 degree increments) were simulated and the results were plotted to observe an effect of the angled beam on heating and production profiles. This particular set of simulations only assumed an angled beam. The center of the beam was still fixed to the center of the front window of the target assembly. These runs were performed for a 20 MeV beam and an enriched  $^{100}\text{Mo}$  target. Heating profile showed very little sensitivity in this range of angles. The total drop in energy deposition was around 1.5%. Production, on the other hand, revealed stronger dependence, but the total drop in  $^{99}\text{Mo}$  production at 7 degree angle was only 5.6%. Differences grow bigger deep inside the target simply due to the fact that an angled beam misses more target material as it travels through. An effect of missing the center of the target by a small amount (1-2 mm) in combination with an angled beam was also studied with a different set of MCNPX runs. The results showed additional 8-10% drop in total production at 7 degree angle with a shifted beam and highlighted the importance of hitting the target in the center. Beam angle studies were also compared to the independent simulations performed at LANL and a good agreement was observed.

#### *Linac upgrade*

New accelerator structures for linac upgrade are produced by MEVEX Corporation (Canada). The upgrade was scheduled for the summer of 2011, but was delayed by three month. First part of the upgrade that includes first accelerating structure (Figure 9), high power loads and RF components have been delivered last week of September. The rest of the upgrade that include second accelerator structure, high power RF windows and circulators will be delivered on December 2011.



**Figure 9.** First accelerator structure during factory acceptance test on September 15, 2011

Irradiation of the  $^{100}\text{Mo}$  target at higher energy would significantly increase the yield of  $^{99}\text{Mo}$ . Beam energy in the range 30-35 MeV seems to be the sweet spot for the  $^{100}\text{Mo}(\gamma,n)^{99}\text{Mo}$  reaction. We are planning to implement an upgrade that will allow us to increase beam energy on the target. The linac upgrade will consist of two accelerator structures. Each accelerator section will consist of 21 accelerating cavities. Each of the accelerator structures will be powered by a separate klystron (there are two existing klystrons at ANL for this purpose). RF power from each klystron will go through a circulator (to protect klystrons from back RF reflection) and through the RF window separating vacuum and  $\text{SF}_6$  filled RF waveguide.

During the preliminary design stage, the following assumptions were made: (1) the total peak microwave power available is 32 MW ( $2 \times 16$  MW), (2) the total average microwave power available is 50 kW, (3) two klystrons are available, (4) the maximum RF pulse width is 6.5  $\mu$ s, (5) the maximum repetition rate is 240 Hz, and (6) the maximum length available for accelerating the structure is 4.8 m. Based on these assumptions, the accelerator structures is expected to be capable of the operating conditions contained in Table 1.

**Table 1.** Operating Conditions of the new Accelerating Structures calculated using following assumptions: RF power 16 MW per accelerating structure, pulse width 4 $\mu$ s, repetition rate 200 Hz.

| Energy (MeV)                          | 15    | 20    | 25    | 30   | 35    | 40    | 45   | 50  | 55  |
|---------------------------------------|-------|-------|-------|------|-------|-------|------|-----|-----|
| Beam Peak Current (mA)                | 1390  | 1230  | 1060  | 900  | 740   | 570   | 390  | 240 | 80  |
| Average Beam Current ( $\mu$ A)       | 1112  | 984   | 848   | 720  | 592   | 456   | 312  | 192 | 64  |
| Average beam power on the target (kW) | 16.76 | 19.64 | 21.32 | 21.6 | 20.66 | 18.28 | 14.2 | 9.6 | 3.6 |

After the installation of the upgrade is complete, ANL's low-energy linac will be able to deliver 21.6 kW of beam power at 30 MeV to study effectively the performance of a target under irradiation in production relevant conditions and will be able to deliver significant beam power to the target at 45 and 50 MeV to study side reactions.

### 3.2. Activities related to the target processing

#### *Dissolution studies in hydrogen peroxide*

Initial dissolution experiments for 12 $\times$ 1mm sintered Mo disks showed that there is a big difference in dissolution rates of disks treated with PTFE (Teflon) used as a releasing agent, which do not dissolve as quickly as disks without PTFE. Some PTFE disks would not dissolve even after several hours. One of the explanations could be that some residues of PTFE were still present after sintering process and could negatively affect the dissolution rates. Comparison between dissolution of some Mo disks is presented in Figure 10.

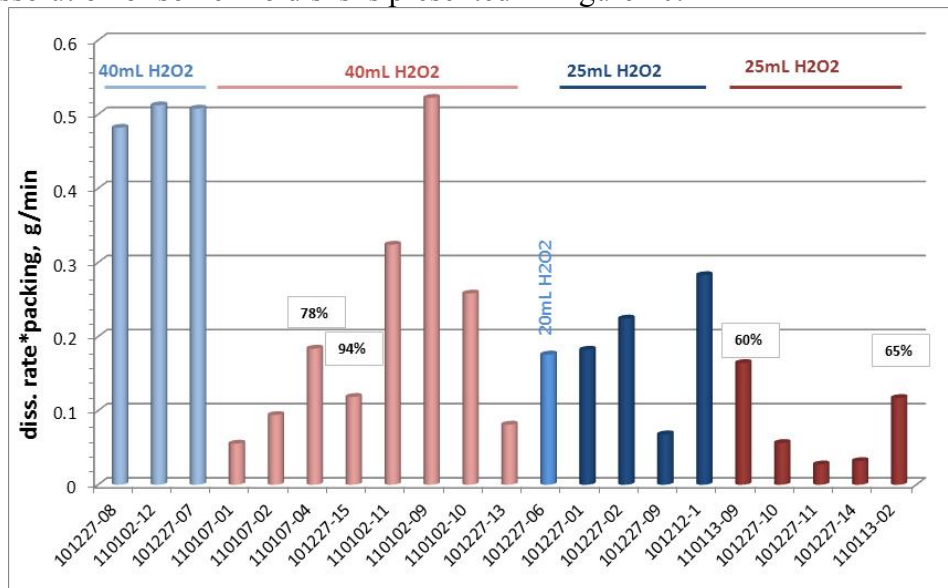


**Figure 10.** Comparison of dissolution rates for some PTFE and non-PTFE disks. Percentage above some bars indicates how many percent of the initial mass were dissolved.

Data in Figure 10 clearly demonstrate slower dissolution rates for PTFE disks. Another important factor that can affect the dissolution rate is initial volume of  $H_2O_2$ . After communication with manufacturer of the disks, the problem with worse dissolution of PTFE discs was eliminated and for the new batch of the Mo disks, no significant difference in the dissolution rates for PTFE and non-PTFE disks was observed.

To better understand the dissolution rates, also Scanning Electron Microscope technique (SEM) was applied. Comparison of the SEM images of the surface of fresh undissolved Mo sintered disk and partially dissolved Mo disk can be seen in Figure 11. SEM images taken from the partially undissolved residues of Mo sintered disks show enormous surface area with lots of small holes, some less than  $1\mu m$  in diameter. A reason for a non-complete dissolution of some disks could be relatively high surface tension of hydrogen peroxide that prevents a good contact with surface of the disk. Therefore, to decrease its surface tension, temperature of  $H_2O_2$  for the dissolution was increased to  $95-100^\circ C$ . All undissolved residues of Mo sintered disks were dissolved. Experiments when the temperature of  $H_2O_2$  during the dissolution was kept at  $\sim 95^\circ C$  confirms that this helps reduce the dissolution time for disks with higher packing density usually to 10-15 minutes per disk.

From many dissolution studies it was observed that the disks with higher packing density dissolve significantly slower than less dense disks. Although this behavior was expected, more detailed study was performed to investigate the dependence of dissolution rate on the packing density of the disks. Several PTFE and non PTFE sintered disks with packing in the range of 56-94% were dissolved. The dissolution rate linearly decreases with packing density up to 88% packing density. In general, no significant difference between dissolution rates for PTFE and non PTFE disks was observed. However, a significant change in the dissolution rates for the disks with densities higher than 88% (both PTFE and non PTFE) was observed (Figure 12).

In order to dissolve the disks with 94% packing density, a solution of hydrogen peroxide was heated up to  $90-95^\circ C$ . These disks dissolved after  $\sim 13$  minutes. Usual dissolution time for disks with packing density  $< 94\%$  in 30%  $H_2O_2$  and starting temperature of  $70^\circ C$  is less than three minutes per disk ( $\sim 1.1g$ ).

To determine the dissolution rate for simultaneous processing of more disks, twelve Mo sintered disks with total mass  $\sim 12.8g$  and densities in the range of 85.6% - 96.8% were dissolved in  $\sim 400$  mL of  $H_2O_2$ . After  $\sim 10$  minutes, eight disks fully dissolved, another three disks dissolved after  $\sim 22$  minutes and the remaining disk fully dissolved after 34 minutes. Since the dissolution slowed down significantly after 10 minutes,  $H_2O_2$  with dissolved Mo was drained, and fresh  $H_2O_2$  was added and heated continuously to  $\sim 95-100^\circ C$  to fully dissolve the remaining disks. It is expected that the last disk that was very hard to dissolve was the disk with the highest packing density. The total dissolution time for  $\sim 12.8g$  of Mo disks was 34 minutes, which gives a dissolution rate of  $\sim 0.38g/min$ . After the dissolution, the excess of hydrogen peroxide was destroyed by heating, and Mo-peroxo species were converted to molybdate by adding KOH. Total processing time for twelve disks was  $\sim 1$  hour.

A few tests with high density disks ( $\sim 92\%$ ) sintered at lower temperature were also performed. Significantly faster dissolution rates were observed. These disks dissolved in about 80 seconds, which is significantly faster than regular sintered disks with similar packing densities. These experiments demonstrate that light sintering of Mo disks, even with relatively high packing density could potentially lead to very fast and consistent dissolution of the disks. However, from the discussion with manufacturer, light sintering could be problematic for the production of larger disks with high density disks ( $\sim 92\%$ ).

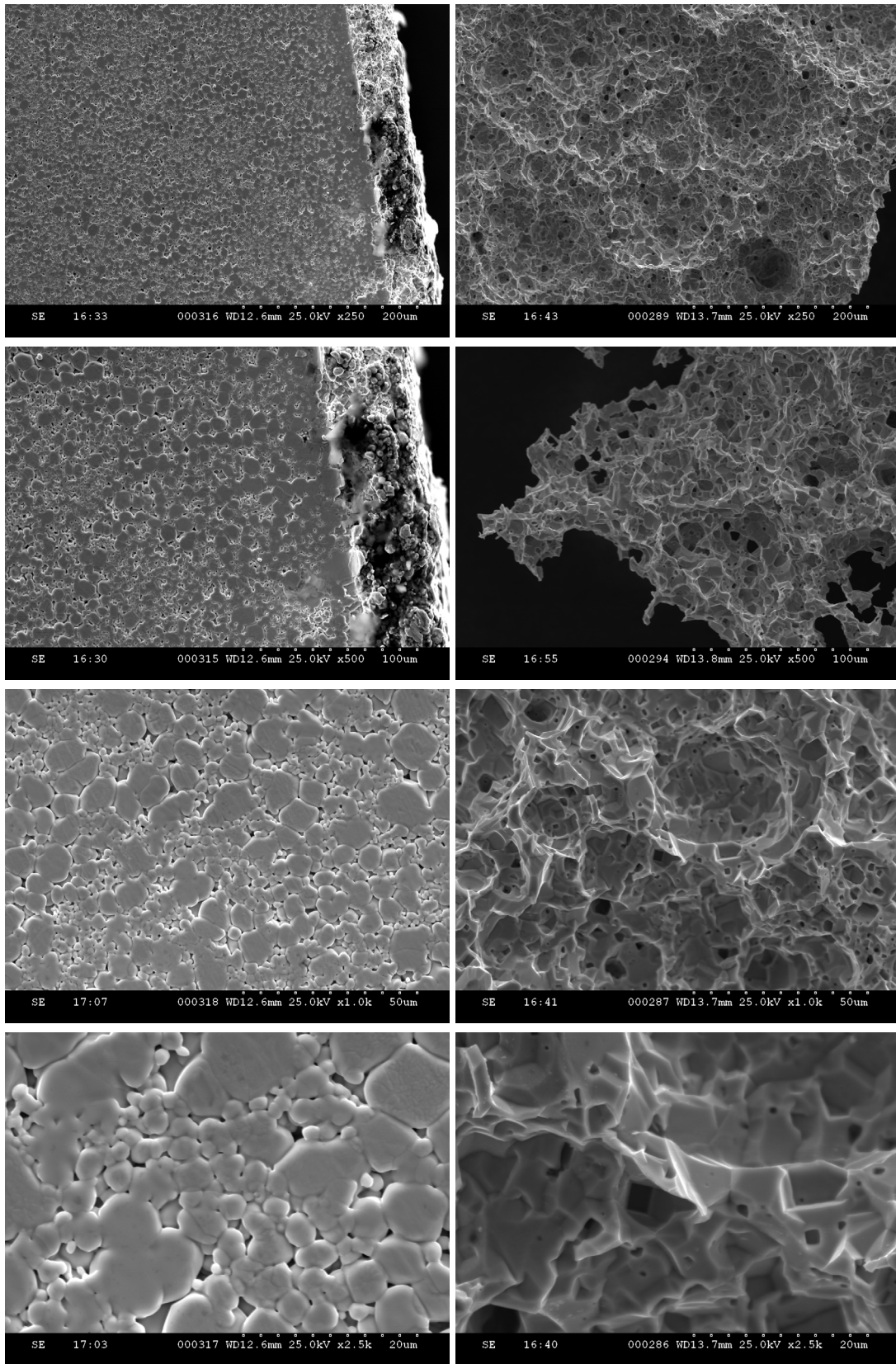


**Figure 11.** SEM images of fresh undissolved (left side) and partially dissolved (right side) 12×1mm Mo sintered disks.

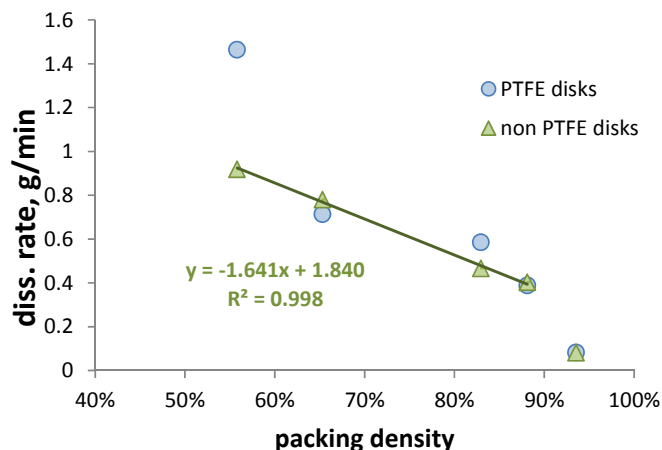


**Figure 12.** Dependence of packing density on the dissolution rate of Mo sintered disks

### *Separation of Mo and Tc*

NorthStar  $^{99}\text{Mo}/^{99\text{m}}\text{Tc}$  generator ARS-II was tested for reproducible recovery of  $^{99\text{m}}\text{Tc}$  in the product vial and to determine if the pH, Mo and Al concentrations in the product solution meet the United States Pharmacopeia (USP) specifications. Distribution of  $^{99}\text{Mo}$  and  $^{99\text{m}}\text{Tc}$  in the throughout the generator was monitored by gamma analysis on the PSC, GC, sterility filter, and in the product and waste solution after every run. Content of Al in the product solution was determined using ICP-MS. Results from the monitoring of  $^{99\text{m}}\text{Tc}$  and  $^{99}\text{Mo}$  activities in the system show that  $\sim 1\%$  of available activity of  $^{99}\text{Mo}$  was lost (mostly to the waste collection vial) after every run. In average, more than 95% of available technetium was consistently recovered in the product vial, which is considerably higher than that achievable by the standard  $^{99\text{m}}\text{Tc}$  generators now being used throughout the world. To control the pH of the saline solution in the Tc product vial, several protocols and gluconate buffer solutions were tested. The protocols were mostly modified in order to control the pH of the product solution by changing the number of washing steps and volume of gluconate buffer. Initial tests have shown high pH of the product solution, which could be due to the presence of small fraction of high pH solution in some part of the generator and affect the pH in the product solution significantly. Control of the pH in the product solution is important also because very strong dependence of aluminum content in the product vial on the pH. This can be clearly seen in Figure 13 that shows the correlation between content of Al and pH in the product solution. After changing the protocol, which added the rinse step and increased the volume of gluconate buffer, the pH and Al content in the product solution dropped significantly. This was further confirmed by additional 10 runs using two different protocols without and with additional rinse step. The concentration of  $^{99}\text{Mo}$  in the product vial determined by gamma analysis and aluminum breakthrough for all samples when the pH of the solution in the product vial was in the range of 4.5–7.5 was below the maximum of the USP specifications. However, due to very low activity of Mo-99 present in the product solutions, the average 1-sigma error for the content of Mo-99 was  $\sim 33\%$ . Future experiments will be performed with higher initial  $^{99}\text{Mo}$  activities to reduce the gamma-counting error to an acceptable level.

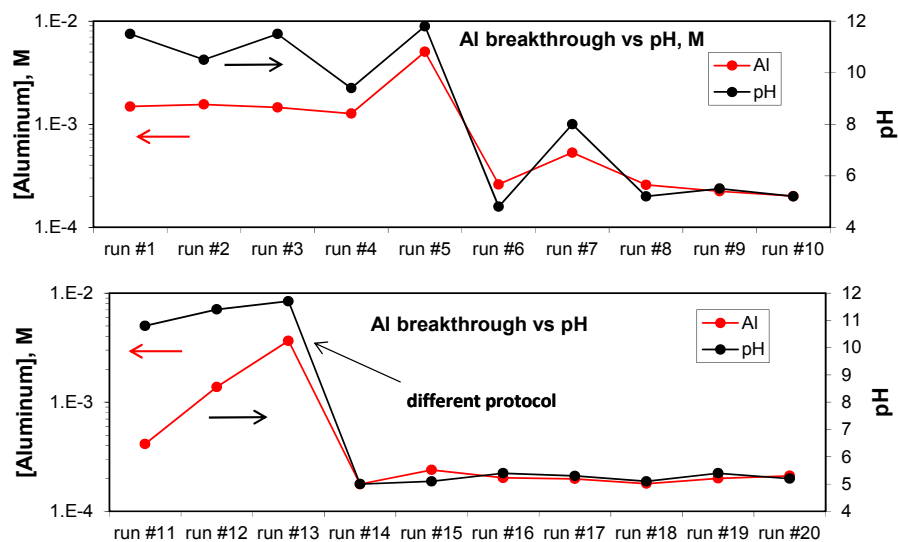


**Figure 13.** Dependence of Al concentration on the pH in the Tc product vial.

#### 4. Conclusions

We designed and analyzed a transport beamline for the two sided irradiations of Mo target at the ANL Linac facility that contains two parallel edge dipoles, one alpha-magnets, two 45-degree magnets and 14 quadrupoles. The quadrupole field strengths were optimized such that the transmission coefficient and the percentage of the beam that is within a 5.0 mm radius circle at the target reach a maximum. It was determined through the simulations that both these parameters are better than 99% when energy spread is 1%. When energy spread is raised to 2% the transmission coefficient is 96% and the beam on target is 86%.

From the dissolution studies performed with more than ninety 12mm×1mm disks it is becoming evident that the packing density and the sintering process are the most significant factors that can considerably affect the dissolution rates. For the higher production of  $^{99}\text{Mo}$ , the disks with higher densities are preferred. However, the data indicate that the dissolution rates can significantly differ for the packing densities in the range of 88-97% and could potentially complicate the post-irradiation processing. Future work will be focused on the dissolution of the disks with high packing density sintered at high and lower temperature. A close cooperation with the manufacturer of the disks and NorthStar to optimize the procedure for disks production is very important and will continue. Using the NorthStar Mo/Tc generator, more than 95% of available technetium was consistently recovered in the product vial, which is significantly higher than using standard  $^{99\text{m}}\text{Tc}$  generators currently being used throughout the world. The product solution also meets the United States Pharmacopeia requirements for pH, and content of molybdenum and aluminum. To increase production of  $^{99}\text{Mo}$  and make future experiments at the linac facility more relevant to planned production facilities, we are proceeding with an energy upgrade that will allow target irradiation at 35 MeV electron beam energy and up to 22 kW total beam power on the target.

#### 5. Acknowledgement

Work supported by the U.S. Department of Energy, National Nuclear Security Administration's (NNSA's) Office of Defense Nuclear Nonproliferation, under Contract DE-AC02-06CH11357. Argonne National Laboratory is operated for the U.S. Department of Energy by UChicago Argonne, LLC.